Sickle cell vasoocclusion and rescue in a microfluidic device

J. M. Higgins*†, D. T. Eddington‡§, S. N. Bhatia‡¶‖, and L. Mahadevan*,**††

*School of Engineering and Applied Sciences, Harvard University, 29 Oxford Street, Cambridge, MA 02138; Departments of †Pathology and ¶Medicine, Brigham and Women's Hospital, Harvard Medical School, 75 Francis Street, Boston, MA 02115; ‡Division of Health Sciences and Technology and ‖Department of Electrical Engineering and Computer Science, Massachusetts Institute of Technology, 77 Massachusetts Avenue, Cambridge, MA 02139; and **Department of Systems Biology, Harvard Medical School, 200 Longwood Avenue, Boston, MA 02115

The pathophysiology of sickle cell disease is complicated by the multiscale processes that link the molecular genotype to the organismal phenotype: hemoglobin polymerization occurring in milliseconds, microscopic cellular sickling in a few seconds or less [Eaton WA, Hofrichter J (1990) *Adv Protein Chem* 40:63–279], and macroscopic vessel occlusion over a time scale of minutes, the last of which is necessary for a crisis [Bunn HF (1997) *N Engl J Med* 337:762–769]. Using a minimal but robust artificial microfluidic environment, we show that it is possible to evoke, control, and inhibit the collective vasoocclusive or jamming event in sickle cell disease. We use a combination of geometric, physical, chemical, and biological means to quantify the phase space for the onset of a jamming event, as well as its dissolution, and find that oxygen-dependent sickle hemoglobin polymerization and melting alone are sufficient to recreate jamming and rescue. We further show that a key source of the heterogeneity in occlusion arises from the slow collective jamming of a confined, flowing suspension of soft cells that change their morphology and rheology relatively quickly. Finally, we quantify and investigate the effects of small-molecule inhibitors of polymerization and therapeutic red blood cell exchange on this dynamical process. Our experimental study integrates the dynamics of collective processes associated with occlusion at the molecular, polymer, cellular, and tissue level; lays the foundation for a quantitative understanding of the rate-limiting processes; and provides a potential tool for optimizing and individualizing treatment, and identifying new therapies.

blood flow | jamming | microfluidics

Sickle cell disease, the first molecular disease to be identified more than a half century ago (1), has been studied extensively at the molecular, cellular, and organismal level. On the one hand, much is known separately about the molecular details of sickle hemoglobin polymerization (2, 3), sickle cell deformability and its effects on flow (4, 5), and the clinical heterogeneity of sickle cell disease (6–9). On the other hand, even though it is perhaps the simplest example of how a physicochemical process at the molecular level leads to pathology at the organismal level, integrating these processes presents a challenge at the intersection of medicine, biology, chemistry, and physics.

At the molecular level, the polymerization of hemoglobin S (HbS) occurs via a double-stranded nucleation mechanism and leads to explosive cooperative growth (3, 9) that depends critically on the ambient partial pressure of oxygen. Polymerization leads to the formation of HbS fibers (2, 8), lowering the oxygen affinity and facilitating the unloading of oxygen into tissue, and thus could provide a physiological advantage. However, polymerization of HbS changes the morphology and stiffness of the red blood cell (8, 10, 11) and thus its ability to flow through the narrowest vessels. In vascular tissue consuming oxygen, the cells slow down, and the local oxygen concentration falls more sharply, leading to further sickling through a positive feedback mechanism and, eventually, jamming of the vessel (termed vasoocclusion) as shown schematically in Fig. 1a. Polymerization and sickling alone have no severe pathophysiolog-

ical consequences, whereas the obstruction of microvessels and the consequent oxygen deprivation of tissue lead to significant disease. Indeed, this jamming of moving particles in a confined environment that occurs in a number of physical processes such as the flow of grains, colloids, and traffic in confined environments (12), where collective effects are crucial in determining the response of the system, is also important in other pathophysiologic processes such as leukostasis in leukemia (13) and hyperviscosity syndrome in multiple myeloma (14). In sickle cell disease, the phenomena just described involve two collective processes at different length and time scales: that of subsecond polymerization and morphological and rheological change at the length scale of an individual cell, and that of collective hydrodynamic flow of a soft suspension of cells that form an occlusive plug the size of an entire confining vessel and slow down over the course of minutes. Therefore, the onset of vasoocclusion is governed by the ratio of two fundamental time scales in the problem (2): the polymerization time, τ_p, for the sickling of a cell in an oxygen-deprived environment, which depends directly on the intracellular concentration of HbS, the local oxygen concentration, and any significant intracellular concentrations of other hemoglobin isoforms such as fetal hemoglobin (HbF); and the kinetic time, τ_k, for blood to transit a narrow long vessel, which depends on the pressure gradient driving the flow, the diameter of the vessel, and the effective viscosity of the blood, which depends on the concentration, shape, and elasticity of the cells it contains. If $\tau_p > \tau_k$, then the deoxygenated blood cell returns to the lungs before sickling, whereas if $\tau_p < \tau_k$, the propensity for polymerization, sickling, and occlusion increases dramatically (3) [see *Qualitative Picture of the Events Leading to an in Vitro Vasoocclusive Event* in supporting information (SI) Text].

The temporal progression of blood flow and occlusion in a vessel is therefore controlled in part by the large-scale pressure gradient, vessel diameter, red cell concentration in the blood (hematocrit), intracellular HbS concentration, and oxygen concentration. We developed a microfluidic device (shown in Fig. 1b) that enables the independent modulation of these parameters to control the onset of vasoocclusion and its reversal. This device allows us to manipulate these geometrical, physical, chemical, and biological determinants and thence parse out the rate limiting processes that govern occlusion and its rescue.

Fig. 1. Schematic of vasoocclusion and experimental setup. (*a*) Multiscale schematic of the collective processes of vasoocclusion: polymerization of HbS occurring at the 10-nm length scale, cell sickling at the 10-μm length scale, and vessel jamming at up to 100 μm. The time scales for the different processes range from a fraction of a second for polymerization to a few minutes before a vasoocclusive event: jamming of the artificial vessel by deformed and rigid red blood cells. (*b*) Fabrication and schematic of the device. The oxygen channels and vascular network were fabricated in separate steps, bonded via oxygen plasma activation, and attached to a glass slide. The widest cross-section in the vascular network on the left and right of the device is 4 mm $\times$ 12 μm. The vascular network then bifurcates, maintaining a roughly equal total cross-sectional area. The gas channels were connected to two rotameters regulating the gas mixture that was fed into the device. The outlet of the gas network had an oxygen sensor to validate the oxygen concentration in the microchannels.

Results

Because vasoocclusion fundamentally represents the inability of the blood to flow, we measured the local velocity of the red blood cells in a microfluidic device with a selected minimal channel width (see SI Movies 1–6). We controlled the pressure difference driving the steady flow of blood using a constant hydrostatic head, and we determined the time for occlusion as a function of ambient oxygen concentration. Because occlusion is a dynamical event, we picked a maximum threshold time for occlusion of 10 min, chosen as an extreme physiological limit. Maximum transit times of red blood cells through individual human vascular beds have been shown to take up to at least 1 min (15). We inflated this time by a factor of 10 to accommodate the possibility of *in vivo* subpopulations with even more extreme transit times and the possibility of traversing multiple vascular beds. These experiments allow us to characterize the phase space of occlusion or jamming using three coordinates: the minimum channel width in the microfluidic device, the total hydrostatic pressure difference across the device, and the ambient oxygen concentration.

Fig. 2 shows a phase diagram where the volume between the coordinate planes and the curved surface shown defines the parameter space where occlusive events would be expected to occur within 10 min. Similar approximately-parallel isosurfaces (not depicted) define the boundary of differing temporal thresholds for occlusion (see SI Movie 7 for three-dimensional visualization). For unaffected individuals with 100% hemoglobin A (HbA), all fixed-time isosurfaces are located very close to the origin because the time to occlusion becomes very large almost regardless of pressure, oxygen, and vessel width (see *Control Experiments with Wild-Type and Sickle-Trait Blood* in SI Text). Conversely, increasing the concentration of HbS yields a phase space with fixed-time isosurfaces farther from the origin, thereby enclosing a wider range of parameter states where occlusion would occur.

Fig. 3a shows that rescue occurs over a much shorter time scale than occlusion. This dynamical asymmetry or hysteresis between occlusion and rescue events is a robust result that occurs in >95% of our experiments. The evolution of the vasoocclusive event was highly stochastic with large variations about the mean time for jamming under a fixed set of control parameters. This heterogeneity could arise from at least two sources: the highly cooperative nature of the HbS polymerization reaction whose onset is very slow relative to the subsequent explosive growth (3, 9), and the hydrodynamics of highly concentrated suspensions that are well known to jam (12, 16). We quantified the degree of hysteresis between the occlusion and rescue events by calculating the ratio between the characteristic time to occlusion (τ_o) and the characteristic time to relaxation (τ_r), defined as the time required to reach half of the maximum velocity. Fig. 3b shows that, as the size of the minimal channel width increases beyond the red blood cell diameter of $\approx$7 μm, there is a significant increase in the variability of this ratio (see *Occlusion and Rescue Hysteresis* in SI Text for more details). In the devices with minimal channel width comparable to the size of a red blood cell, the ratio of the characteristic time to occlusion to that for rescue is more consistent across experiments. The effect of a sudden decrease in deformability caused by deoxygenation and polymerization alone is not sufficient to initiate an occlusive event in all but the narrowest channels; in addition, one needs multiple cells to form a stiff percolating network across the channel before there is a significant reduction in the velocity of the blood leading to vasoocclusion and self-filtration of the plasma. The large variability in the characteristic occlusion times in larger channels, as seen in Fig. 3b, is a signature of the stochastic nature of the percolating process.

Whereas jamming is a collective event, unjamming is not, because oxygen diffuses rapidly through the channels so that the intracellular HbS fibers depolymerize, making the cells more deformable fairly quickly ($\approx$10 sec), and flow starts. We expect to see less variability in the characteristic time for relaxation regardless of minimal channel size, again consistent with our experiments (see *Occlusion and Rescue Hysteresis* in SI Text). Because the polymerization processes typically occur in a few milliseconds when oxygen is quenched rapidly and are thus much faster than the flow processes leading to jamming that take hundreds of seconds, this hysteresis points to the crucial role of the hydrodynamics of the suspension of red blood cells in plasma as the rate-limiting step in the occlusive event in our microfluidic chip.

We next used our device to compare the flow velocity profiles of a patient sample before and after red cell exchange (or erythrocytapheresis), an established clinical procedure in which a sickle cell patient's blood is partially replaced with donor HbA-containing red blood cells. Fig. 4a quantifies the efficacy of the actual medical treatment of a patient with sickle cell disease: velocity of the treated specimen declines much more slowly after deoxygenation, and there is no actual occlusion. This assay could be used to help determine the optimal HbS fraction and

Fig. 2. Phase space of vasoocclusion. The surface represents a fitted hypersurface in four-dimensional space: width, pressure, oxygen concentration, and occlusion time. The isosurface was computed from 43 data points by using Delaunay triangulation [see the MATLAB *griddata3* function documentation (MathWorks)]. All points on the hypersurface correspond to triples of width, pressure, and oxygen concentration where the fitted time to occlusion was 500 sec. The color of each point on the surface characterizes the minimal width in the device and is redundant with the point's vertical (width) coordinate. Pressures were normalized for hematocrit and for individual device resistance (see *Pressure Normalization* in *SI Text*). The filled contour plots represent slices through the fitted volume at specific planes (*Top*, oxygen concentration = 0.5%; *Middle*, normalized pressure = 20 cm H_2O; *Bottom*, minimal width = 25 μm). This phase space describes the behavior of patient samples with a HbS fraction of at least 65% (mean 86%, standard deviation 6.7%). The stochasticity in the vasoocclusive event leads to large variations about the mean time for jamming. We characterize the deviations from the mean time to occlusion by $X = 1/n \sum |t_{\text{fit}} - t_{\text{actual}}|/t_{\text{actual}}$. We find that X is 46%; i.e., vasoocclusion is highly heterogeneous temporally. See SI Movie 7 for a three-dimensional visualization.

hematocrit targets for the exchange procedure, and these optimal treatment goals could be individualized for each patient.

Finally, we investigated the impact of small-molecule inhibitors of polymerization. Carbon monoxide (CO) binds to hemoglobin at least 200 times more tightly than does oxygen and utilizes the same binding site, thus inhibiting polymerization (3). The velocity profiles in Fig. 4*b* show that small concentrations of CO (0.01%) are sufficient to prevent an occlusion even when the ambient oxygen concentration is 0%. We also evaluated the effect of two solid small molecules, phenylalanine and a 2,3-diphosphoglycerate analog. These molecules did not cause a significant change in occlusion profiles [see *Effect of Phenylalanine and Pyridoxal (a 2,3-Diphosphoglycerate Analog) on Occlusive Events* in *SI Text*], but these studies demonstrate the potential use of this device to identify novel treatments for sickle cell disease.

Discussion

Our studies show that the vasoocclusive pathophysiology of sickle cell disease can be captured in a minimal microfluidic environment by using a variety of geometrical, physical, chemical, and biological controls. While adhesion, endothelial phenotype, inflammation, etc., are likely to be contributors *in vivo*, we have highlighted the role of collective macroscopic suspension hydrodynamics on occlusive events, and our phase diagram quantifies the parameter space associated with a potential occlusion by integrating the evolution of HbS polymerization, the change in the shape and elasticity of individual red blood cells, and their collective flow properties. Repeated cycles of sickling on larger time scales *in vivo* may lead to endothelial and inflammatory responses (17, 18) and cause additional positive

feedback; however, as we show, it is possible to evoke and revoke an occlusive event in a minimal physiologically relevant system that does not require these processes to be at work.

From a scientific perspective, the collective jamming seen in physical and social dynamical systems such as the flow of grains, suspensions, and traffic have biological analogs in vasoocclusion, as we have shown, but are also likely to be relevant to platelet aggregation, malarial cell sequestration, lipid jamming in bilayers, etc. (11), where we have to consider events at multiple scales. From an engineering perspective, our minimal microfluidic environment also provides a context in which we can study a variety of blood flow problems (19, 20) and is easily modified to account for complex flow geometries and the incorporation of adhesion molecules (21) and, eventually, endothelial cells. From a clinical perspective, our device allows us to measure the efficacy of treatments at the level of the individual patient by quantifying the propensity for vasoocclusion in terms of the phase diagram in Fig. 2 and thus to determine optimal hematocrit and HbS fractions individualized for sickle cell patients undergoing red cell exchanges and also guide prophylactic treatments in special medical situations including pregnancy (22) and elective surgery (23). Additionally, this device allows for the assessment of the dynamical efficacy of different regimens of traditional drugs such as hydroxyurea (24, 25). Our microfluidic chip also provides a tool for novel treatments of this crippling disease, including possible agents that partially and dynamically inhibit polymerization sufficiently to prevent vasoocclusion without permanently binding to hemoglobin (10).
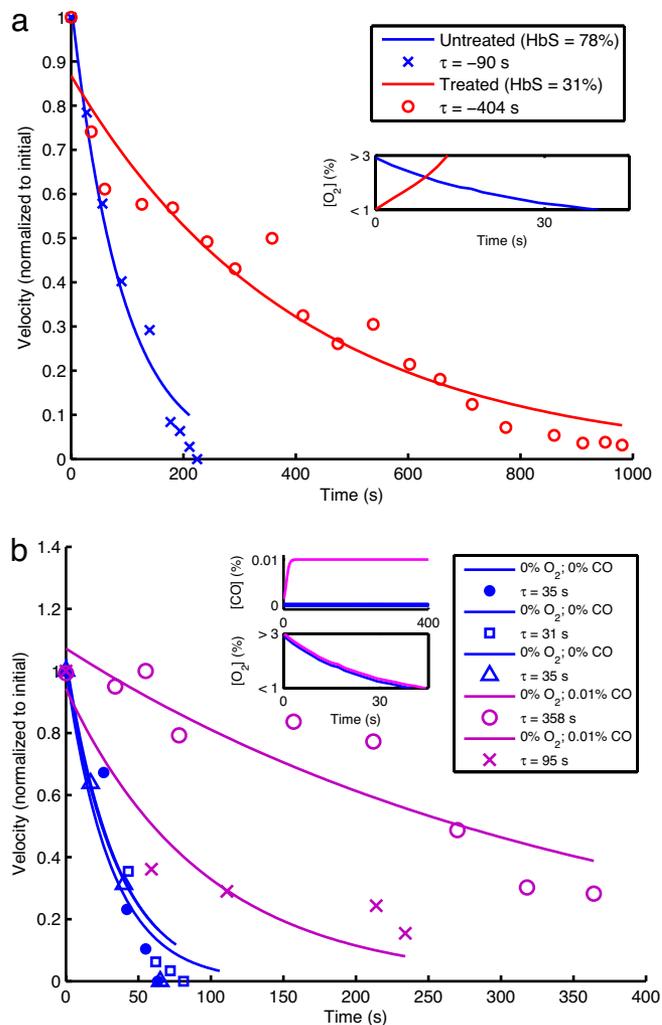
Methods

Blood Specimens. Blood specimens were collected during the normal course of patient care at Brigham and Women's Hospital and used in experiments in
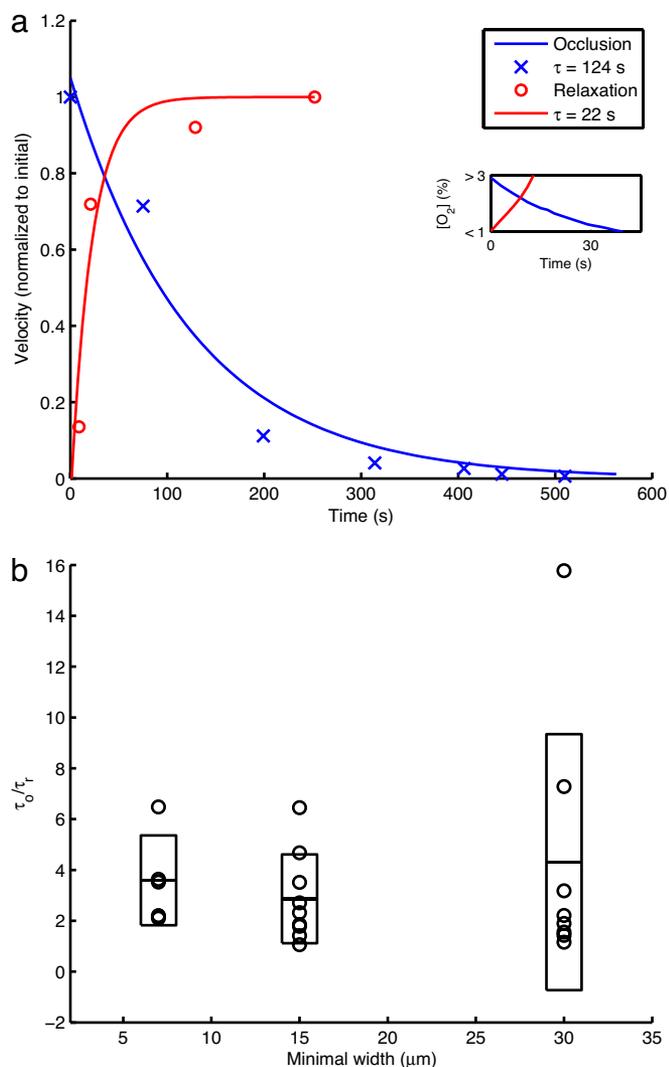
Fig. 3. Occlusion and relaxation and their hysteresis. (*a*) Velocity profiles for an occlusion and relaxation assay for a device with a minimal width of 30 μm and a blood sample with 92% HbS. Data points represent measured velocities normalized to the maximum within each assay. Lines represent least-squares exponential fits. The occlusion measurements had a time scale of $\approx$124 sec, whereas the corresponding time scale fit to the relaxation profile was $\approx$22 sec. We note that the velocity of the red blood cells actually does vanish on occlusion. (*Inset*) Oxygen concentration profiles as measured during a control experiment detailed in *Methods*. Our velocity profile measurements begin with measurable changes in velocity that will occur when intracellular oxygen concentration drops below 3% or rises above 1% (see *Methods* for more details). (*b*) Ratios of characteristic occlusion and relaxation times for occlusion and relaxation assays in devices with different minimal widths. The circles represent individual data points (five at 7 μm, nine at 15 μm, and eight at 30 μm). The horizontal bars represent sample means. The rectangles represent the extent of the mean ± sample SD. For more details, see *Occlusion and Rescue Hysteresis* in *SI Text*.

Fig. 4. Effect of perturbations on occlusion. (*a*) Velocity profiles for occlusion of a patient blood sample before and after therapeutic red blood cell exchange as measured in a device with a minimal diameter of 30 μm and ambient oxygen concentration that is suddenly reduced to 0%. Velocities are normalized to the maximum within each assay. The blue data points represent the behavior of the patient's sample before treatment (78% HbS). The red data points represent the behavior of a sample obtained after treatment (31% HbS). The lines represent least-squares exponential fits. Note that the velocity of the untreated specimen vanishes after a finite time, whereas that of the treated specimen never vanishes. (*Inset*) Oxygen concentration profiles as measured during a control experiment detailed in *Methods*. (*b*) Velocity profiles for occlusion with and without carbon monoxide. All assays were carried out in a device with a minimal diameter of 15 μm and a patient blood sample with 85.5% HbS. The blue markers correspond to three different occlusion assays with no oxygen or carbon monoxide. The purple markers correspond to assays with 0.01% carbon monoxide and 0% oxygen. (*Insets*) Gas concentration profiles, with *Lower Inset* reflecting control measurements detailed in *Methods*.

accordance with a research protocol approved by the Partners Healthcare Institutional Review Board. Blood samples were collected in 5-ml EDTA vacutainers and stored at 4°C for up to 60 days. Hematocrit was determined using a Bayer ADVIA 2120 automated analyzer. Hemoglobin fractions were determined using cellulose agar electrophoresis and confirmed by HPLC with a Tosoh G7 column.

Fabrication of Microfluidic Devices. The multilayered microfluidic network was fabricated in poly(dimethylsiloxane) (PDMS) by using previously described soft lithography techniques (26). The multilayered device consists of a 150-μm-thick gas channel network separated from a 12-μm vascular network by a

150-μm PDMS membrane. An SU8 photoresist (Microchem) was used to fabricate the mold masters for both the vascular and gas channels. The vascular network was fabricated to be 12 μm thick by spin-coating SU8–2015 onto a 4-inch silicon wafer at 3,000 rpm for 30 sec. This wafer was then softbaked at 65°C for 1 min and 95°C for 2 min. Next, the SU8-coated substrate was placed into soft contact with a high-resolution transparency photomask and exposed with UV light (365 nm) at 100 mJ/cm^2. This substrate was then hardbaked at 65°C for 1 min and 95°C for 2 min to complete the cross-linking process. The wafer was allowed to cool to room temperature and developed in SU8 developer (Microchem). The gas channels were fabricated to be 150 μm thick through similar techniques, with the exception of slower spin velocity (1,200 rpm), longer softbakes (65°C for 7 min and 95°C for 60 min), more

energy for exposure (400 mJ/ cm²), and a longer hardbake (65°C for 1 min and 95°C for 15 min).

Once the mold masters were fabricated, PDMS (SYLGARD 184; Dow Corning) was prepared by mixing the PDMS prepolymer and cross-linker in a 10:1 ratio, degassing for 1 h to remove air bubbles, and curing at 75°C for 90 min. The assembly of the device is shown in Fig. 1b. The 150-μm-thick PDMS membrane was patterned with the vascular network by first pouring 5 ml of PDMS onto the vascular network mold master. Next, a transparency was placed onto the PDMS to facilitate removal from the 4-inch glass plate that was used to ensure a uniform pressure distribution over the mold master. Finally, 500 g of compression weights were placed onto the glass plate. The 150-μm gas channel network was molded in a 5-mm-thick block of PDMS with holes for tubing connections cored with a 12-gauge syringe needle. The patterned PDMS membrane was first bonded to the gas channel network and then bonded to a glass slide by using an oxygen plasma system (PlasmaPreen; Terra Universal) to activate the surfaces before bonding. After bonding, the devices were placed in an oven at 75°C overnight to improve bonding strength and stabilize material properties (27). The bonded devices were placed in a dessicator for 5 min before filling to reduce bubble formation. The devices were first filled with water to facilitate the use of high pressures to drive out the remaining air bubbles without the risk of dealing with potentially infectious human blood samples under high pressures. Once the device was initially primed with water, blood was easily injected into the device by using gravity-driven flow.

Experimental Setup. The assembled microfluidic device was mounted on an inverted microscope (Nikon TE-3000), and the fluidic and gas sources were connected as shown in Fig. 1b. The microfluidic channels begin 4 mm wide, then split into roughly equal total cross-section areas until the smallest dimension (7, 15, 30, or 60 μm), which then traverses 4 cm until the channels recombine sequentially at the outlet. The blood velocity was monitored most often in the 250-μm channels, which were fed by four 60-μm, eight 30-μm, sixteen 15-μm, or sixteen 7-μm channels, depending on the device studied. Two rotameters controlled the gas mixture fed through the oxygen channels. The gas mixture diffused rapidly through PDMS to initiate occlusion or flow. The outlet gas concentration was monitored with a fluorescent oxygen probe (FOXY fiber optic oxygen sensor; Ocean Optics) to monitor the gas concentrations within the gas microchannels. Gravity-driven flow was used to inject blood into the vascular network and resulted in flow rates of up to 500 μm/sec.

We performed >100 different such occlusion assays, capturing >1,000 videos with >100,000 total frames. Given a device with a particular minimal width (7, 15, 30, or 60 μm), we flowed a patient blood specimen with a known HbS fraction and a known red blood cell concentration. We modulated the pressure difference by changing the height of the pressure head and modulated the gas concentration in the fluid channel by adjusting the gas mixture flowing through the adjacent gas channels. Videos were captured at intervals.

Oxygen Diffusion into Microchannels. We find that oxygen diffuses through our experimental device over time scales on the order of 10 sec (roughly 10 times faster than occlusion and rescue events, which occur over time scales on the order of 100 sec). The oxygen concentration within the vascular network was quantified through bonding the microfluidic network to a glass slide coated with a ruthenium complex (FOXY-SGS-M; Ocean Optics) that fluoresces under 460-nm excitation and is quenched by oxygen. The intensity of the fluorescence can be correlated to the oxygen concentration by using the Stern–Volmer equation (28).

It is important to consider the relative rates of ambient deoxygenation and hemoglobin oxygen unloading, especially when the collective chemical polymerization and collective hydrodynamics can act in concert. We expect the diffusion times for water-filled fluid channels in our control experiment to be similar to those for blood-filled channels because the fluid channel itself is 12 μm (or a few cells) high and represents only 10% of the total diffusion distance, which includes a 100-μm-thick PDMS membrane between the gas and fluid channels (see SI Fig. 9). Our velocity profile measurements begin with measurable changes in velocity that will occur when intracellular oxygen concentration drops below 3% or rises above 1%. Very rapid polymerization will occur when this concentration is below 1–2%.

Data Collection and Analysis. Assays were performed at room temperature. Videos were captured with a PixeLINK PL-A781 high-speed video camera. Videos were processed and analyzed using MATLAB, the MATLAB Image Processing Toolbox, and the Simulink Video and Image Processing Blockset (MathWorks).

1. Pauling L, Itano HA, Singer SJ, Wells IC (1949) *Science* 110:543–548.
2. Eaton WA, Hofrichter J (1990) *Adv Protein Chem* 40:63–279.
3. Mozzarelli A, Hofrichter J, Eaton WA (1987) *Science* 237:500–506.
4. Gregersen MI, Bryant CA, Hammerle WE, Usami S, Chien S (1967) *Science* 157:825–827.
5. Alexy T, Pais E, Armstrong JK, Meiselman HJ, Johnson CS, Fisher TC (2006) *Transfusion* 46:912–918.
6. Serjeant G, Serjeant B (2001) *Sickle Cell Disease* (Oxford Univ Press, Oxford).
7. Bunn HF (1997) *N Engl J Med* 337:762–769.
8. Ballas SK, Mohandas N (2004) *Microcirculation* 11:209–225.
9. Ferrone FA (2004) *Microcirculation* 11:115–128.
10. Cohen AE, Mahadevan L (2003) *Proc Natl Acad Sci USA* 100:12141–12146.
11. Chien S, King RG, Kaperonis AA, Usami S (1982) *Blood Cells* 8:53–64.
12. Liu AJ, Nagel S, eds (2001) *Jamming and Rheology* (Taylor and Francis, London).
13. Porcu P, Cripe LD, Ng EW, Bhatia S, Danielson CM, Orazi A, McCarthy LJ (2000) *Leuk Lymphoma* 39:1–18.
14. Rampling MW (2003) *Semin Thromb Hemostasis* 29:459–465.
15. MacNee W, Martin BA, Wiggs BR, Belzberg AS, Hogg JC (1989) *J Appl Physiol* 66:844–850.

16. Berger SA, King WS (1980) *Biophys J* 29:119–148.
17. Fabry ME, Fine E, Rajanayagam V, Factor SM, Gore J, Sylla M, Nagel RL (1992) *Blood* 79:1602–1611.
18. Gimbrone MA, Jr, Topper JN, Nagel T, Anderson KR, Garcia-Cardena G (2000) *Ann NY Acad Sci* 902:230–239; discussion 239–240.
19. Runyon MK, Johnson-Kerner BL, Ismagilov RF (2004) *Angew Chem Int Ed* 43:1531–1536.
20. Whitesides GM (2006) *Nature* 442:368–373.
21. Makamba H, Kim JH, Lim K, Park N, Hahn JH (2003) *Electrophoresis* 24:3607–3619.
22. Koshy M, Burd L, Wallace D, Moawad A, Baron J (1988) *N Engl J Med* 319:1447–1452.
23. Vichinsky EP, Haberkern CM, Neumayr L, Earles AN, Black D, Koshy M, Pegelow C, Abboud M, Ohene-Frempong K, Iyer RV (1995) *N Engl J Med* 333:206–213.
24. Hankins JS, Ware RE, Rogers ZR, Wynn LW, Lane PA, Scott JP, Wang WC (2005) *Blood* 106:2269–2275.
25. Nathan DG (2002) *J Pediatr Hematol Oncol* 24:700–703.
26. Duffy D, McDonald J, Schueller O, Whitesides G (1998) *Anal Chem* 70:4974–4984.
27. Eddington DT, Puccinelli JP, Beebe DJ (2006) *Sens Actuators B* 114:170–172.
28. Evans RC, Douglas P (2006) *Anal Chem* 78:5645–5652.